IEEE Access
Multidisciplinary | Rapid Review | Open Access Journal

Received April 22, 2020, accepted May 31, 2020, date of publication June 8, 2020, date of current version June 18, 2020.

Digital Object Identifier 10.1109/ACCESS.2020.3000604

Multilevel High-Rate Coding With Twofold Concatenation for IoTs in Wireless Mesh Networks

SHANG-CHIH MA[1], (Member, IEEE), MOHAMMAD ALKHALEEFAH[1], (Member, IEEE), YANG-LANG CHANG[1], (Senior Member, IEEE), LENA CHANG[2], (Member, IEEE), AND BORMIN HUANG[3]

[1]Department of Electrical Engineering, National Taipei University of Technology, Taipei 10608, Taiwan
[2]Department of Communications and Guidance Engineering, National Taiwan Ocean University, Keelung 20248, Taiwan
[3]School of Information Science and Technology, Southwest Jiaotong University, Chengdu 611756, China

Corresponding author: Yang-Lang Chang (ylchang@ntut.edu.tw)

This work was supported in part by the Ministry of Science and Technology, Taiwan, under Grant MOST 108A27A, Grant 108-2116-M-027-003, and Grant 107-2116-M-027-003, in part by the National Space Organization, Taiwan, under Grant NSPO-S-108216, in part by the Sinotech Engineering Consultants Inc., under Grant A-RD-I7001-002, and in part by the National Taipei University of Technology under Grant USTP-NTUT-NTOU-107-02, Grant NTUT-USTB-108-02, and Grant NTUT-UM-109-01.

ABSTRACT Recent studies have shown that wireless mesh networks (WMNs) can be cheap, reliable, and efficient solutions for Internet of Things (IoTs) applications and connected devices. However, the increase in the size of the WMNs could lead to a degradation in performance. This makes the network vulnerable to high error rates over noisy and fading channels. This has increased the demand for more efficient channel coding schemes that can provide reliability, high data rate, high coding gain, energy efficiency, and minimum decoding complexity especially for low-cost and special purpose WMNs. In this research, an original multilevel coding with twofold concatenation scheme is designed based on high-rate space-time block codes (HRSTBCs) to cope with this increasing demand, particularly in MIMO-based WMNs. First, a multilevel coding scheme is implemented by correlating HRSTBCs with the uniquely constructed set-partitioning of the transmission matrix, based on the coding gain distance (CGD) criterion. This generates a new scheme, namely multilevel high-rate space-time block code (MHRSTBC), to provide a high transmission rate. Second, a twofold concatenation coding scheme is introduced by concatenating Reed-Solomon (RS) code, has been used for its energy efficiency and optimality in the mobile environment, with the inner code of the associated MHRSTBC. This has formed a new scheme that reaches the maximum coding gains, called the Reed-Solomon multilevel high-rate space-time block code (RS-MHRSTBC). The efficiency of the RS-MHRSTBC is verified by a computer simulation over a Rayleigh flat-fading and additive white Gaussian noise (AWGN) channel. The RS-MHRSTBC is compared with the classical schemes of Alamouti STBC and Multilevel STBC over uncoded QPSK, and the RS-MHRSTBC shows significant high coding gains reached of 47.79 dB, while Alamouti STBC and Multilevel STBC reached 38.12 dB and 44.30 dB at a BER of 10^{-6} respectively. RS-MHRSTBC also shows a reasonable decoding complexity while maintaining full transmission diversity at spectral efficiency of 2 bits/s/Hz.

INDEX TERMS Channel coding, Internet of Things, Reed-Solomon codes, space-time block codes, wireless network.

I. INTRODUCTION

The recent popularity of the wireless mesh networks (WMNs) is mainly driven by the emergence of IoTs applications and ubiquitous connected devices. WMNs can provide IoTs with a variety of advantages such as seamless coverage, reliability, compatibility, scalability, and security [1]. Smart cities, smart industry, autonomous transportation, and smart healthcare are just some of the examples of IoTs applications that can be empowered by the support of the WMNs [2]–[4]. WMNs

The associate editor coordinating the review of this manuscript and approving it for publication was Ghufran Ahmed.

can be easily configured to suit low, moderate, and high bandwidth IoTs applications. WMNs consist of mesh clients, mesh routers, and gateway to provide internet connectivity to the mesh clients or IoTs devices. Mesh clients can be either fixed or mobile. Mesh nodes or wireless routers which are relatively cheap, can be deployed over a small area, such as an office building, or a large area, such as a city [5]. WMNs nodes rely on the common Wi-Fi communication family of IEEE standards known as 802.11 to communicate on more bandwidth and power. On the other hand, IEEE standards 802.15.4 offers a low-bandwidth and low-cost communication between the ubiquitous IoTs devices [6]. WMNs can be an alternative to a centralized administration, every device can be connected to every other device in a direct or indirect way, therefore there is no single point of failure. WMNs are considered to be self-healing and self-configurable. If one node fails, the network will continue to operate since there are multiple ways to send data across the WMN. In addition, one node can be easily and automatically integrated into the data transmission paths by the advanced WMN routing protocols. WMNs can host their own servers, therefore IoTs connected devices can communicate across the mesh network without being connected to the internet [7]. In addition, WMNs can also be useful in countries that are prone to natural disasters and internet shutdowns. According to Cisco's annual visual networking index forecast, the number of IoTs connected devices will reach 14.7 billion by 2023 [8]. The idea behind IoTs is to enable the physical objects to communicate and exchange data using wired or wireless technologies to provide a certain functionality [9], [10].

In the wireless communications, as the domain of this research, the physical objects connect to one another via some sort of low or high power-range wireless technologies such as, but not limited to, Bluetooth and cellular respectively. Studies recorded that the throughput performance of the WMNs drops dramatically as the number of IoTs devices and nodes increases especially in applications such as a smart city where a multi-hop is required in order to deploy a large and effective WMN for IoTs devices in an interfering and multipath fading environment [5], [11]. In this research, we designed an efficient, simple, and cost-effective channel coding scheme to improve the IoTs devices communication over WMNs by improving the bit error rate (BER) and consequently reducing the total number of data transmissions, which can thus reduce the power consumption and end-to-end delay. The rest of the paper is organized as follows. Section II presents some related works. Section III describes the set-partitioning of the transmission matrix. Section IV demonstrates the multilevel concatenated coding scheme. Section V illustrates the design of the proposed twofold concatenated scheme. Section VI summaries the simulation results. Finally, the research is concluded in Section VII.

II. RELATED WORKS

Multiple-Input Multiple-Output (MIMO) is still the key technology used in wireless communication systems including WMNs. MIMO system can achieve full diversity through the use of multiple transmitters and receivers in order to transfer multiple streams of data at the same time. The concept of diversity in wireless communication systems can be used to provide reliability, reduce the transmitting power, increase data throughout, avoid error bursts, and overcome the effect of fading due to the multipath of the propagated signals in the wireless communication channels [12]. High-rate wireless communication channels may vary as a function of space and time [13]. Tarokh *et al.* [14] proposed the space-time trellis coding (STTC) which is an effective and reliable technique to achieve maximum transmit diversity over fading channels. In STTC, data is encoded by a channel code and encoded by the maximum-likelihood (ML) decoding technique. STTC provides the best theoretical trade-off between diversity gain, transmission rate, constellation size, signal space dimension, and trellis complexity over fading channels using multiple transmit antennas. The performance of the proposed codes was excellent and the decoding complexity was reasonable. Nevertheless, the decoding complexity of STTC increases exponentially as a function of the transmission rate and the diversity level when the number of transmit antennas is fixed.

In order to address the issue of the decoding complexity, Alamouti [15] presented a simple and practical two-branch transmit diversity scheme which is a special case of the space-time code for wireless communication systems. Although the transmission scheme of Alamouti is for multiple-input single-output (MISO) systems, the scheme can be generalized to 2 transmit antennas and 2 receive antennas to provide diversity in MIMO mode. This is done without any channel state information from the receiver to the transmitter and with small computation complexity. The new transmit diversity scheme can reduce the BER at a particular signal-to-noise ratio (SNR) in wireless communications systems. However, there is a loss in performance compared to space–time trellis codes. Despite the complexity of Alamouti's scheme that increases exponentially with the data transmit rate, it is still less complex than STTC for two transmit antennas as it divides the signals transmitted from the two transmit antennas. Tarokh *et al.* [16] used the principle of the space-time block codes (STBCs) to obtain full diversity for a multiple transmit antennas communication system over a fading environment. The STBCs were constructed using the mathematical framework of the orthogonal designs. Authors created analog of Alamouti scheme for more than two transmit antennas. Data is encoded using STBC and decoded by linear processing maximum likelihood. However, a large number of transmit antennas have to be employed to achieve high diversity.

Several STBC schemes have been proposed in the literature to address the open problems of diversity gain, maximum likelihood decoding complexity, and coding gain in MIMO systems [13]–[19]. However, this study focuses on improving the data rate, coding gain, and energy efficiency in WMNs by implementing an efficient and low-cost coding scheme high-rate STBCs and MIMO over Rayleigh fading and additive

white Gaussian noise (AWGN) channels to further empower the communication of the IoTs connected devices and applications. Nevertheless, there are some interesting coding mechanisms designed for improving the performance and coding gain of the WMNs. One study has been reported on improving the throughput of WMNs by applying a localized coding-aware opportunistic routing mechanism [20]. In the coding-aware routing protocol design, there are two fundamental aspects: 1) coding condition, which is used to find the coding opportunities, and 2) routing metric, which should carefully be designed to enhance the routing protocol in an effective way. Nevertheless, the existing localized network coding mechanisms only adopt best path routing and passively wait for the appearance of coding chances on the path which limits the network resources from achieving high performance. Another study [21] proposed COPE, a new practical forwarding architecture that improves the throughput of stationary WMNs by integrating localized network coding mechanism supporting efficient unicast communication and opportunistic forwarding in WMNs. COPE incorporates three essential techniques; opportunistic listening, opportunistic coding, and learning neighbor state. COPE takes advantage of the broadcast nature of the wireless channel and allows nodes using opportunistic listening to get the information from their neighborhood nodes to decide the coding opportunity. It chooses data from the packets to encode, then implement the opportunistic routing. In COPE, all the encoding and decoding operations can be performed using a simple XOR operation. However, the throughput improvements depend on the traffic pattern, and coding structure is restricted to a two-hop route.

Coding-aware opportunistic routing and encoding (CORE) scheme [22] is another opportunistic routing (OR) protocol that exploits the network coding mechanism to improve the throughput of MWNs by utilizing an inner-flow coding technique. As an OR protocol, packets of multiple flows are coded together and transmitted to the candidate nexthops through a consideration of the coding gain that it may achieve. The source sends packets that can be encoded with other packets. The candidates then coordinate among themselves to choose one node as the next forwarder. The decision is made to consider the coding possibility at each node. The packets are forwarded in this manner until they reach the destination. COPE and CORE utilize inter-session network coding to improve the throughput performance of WMNs. However, the previous work has improved the WMNs performance by focusing on improving the routing protocols and channel coding. Unfortunately, these WMNs encoding techniques and routing protocols are complex and did not consider the physical characteristics of the wireless channels such as noise and fading which could cause a degradation in performance and end-to-end delay.

Several promising channel coding designs for wireless communication systems are well presented in [23], [24], including the variants of physical-layer network coding-aided wireless communications and root protograph (RP) codes

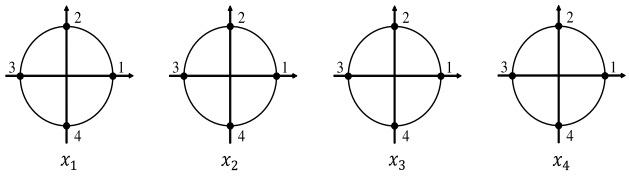

FIGURE 1. The 4 × QPSK signal constellation set.

which belong to the novel family of protograph low-density parity check (LDPC) codes, over block-fading (BF) channels. Readers are advised to read these references for a comprehensive survey of the latest research advancements in channel coding designs [23]–[25]. In many cases, IoTs devices are battery powered and may need to be deployed in some remote and harsh areas where a power source is not available. Therefore, a crucial demand for efficient IoTs-based devices communication exerts pressure on the existing wireless communication infrastructures including WMNs in terms of improving the data transmission and power consumption. Various codes have been studied to assess their potentials for wireless sensor networks (WSNs), including polar codes [26], turbo codes [27], BCH codes [28], LDPC [29], and Reed-Solomon codes [30]. However, Reed-Solomon codes have shown a good trade-off between energy efficiency and coding gains for wireless networks as presented in [31], [32]. The special structure of Reed-Solomon codes can greatly reduce the probability of bit error rate and the computational effort, therefore the target bit error rate with a lower transmitter output power can be achieved. Reed-Solomon codes are very reliable error control codes especially in the wireless communications which are usually affected by channel fading and noise [33]–[35]. Hence, Reed-Solomon is adopted as an outer code in this paper.

In this research, we present a candidate low-cost channel coding scheme that can support MIMO based WMNs-IoTs devices and applications in terms of low BER, robustness, reliability, and efficiency with average rate of 2 bits/symbol using 2×2 antennas over Rayleigh fading and AWGN channel. Unlike other work, we apply MHRSTBC over Rayleigh fading and AWGN channels to produce a powerful scheme that can improve the performance of the IoTs ubiquitous devices communication and applications on top of WMNs. First, a λ-level partition chain $P(\lambda) = W^{(0)}/W^{(1)}/\ldots/W^{(\lambda)}$ of transmission matrix set in the high-rate space-time block codes is constructed. Second, several component codes are combined with the constructed set-partitioning to form the multilevel HRSTBCs scheme after mapping it with a $4\times$ quadrature phase-shift-keying (QPSK) signal set. Finally, the multilevel HRSTBCs scheme is further concatenated with an outer Reed-Solomon code to maximize coding gains and avoid large decoding complexity of long codes over AWGN and Rayleigh fading channels.

The set-partitioning technique might not be new, however, the five-level binary partition tree 2^5 that is introduced in this paper is unique and original. In addition, combining

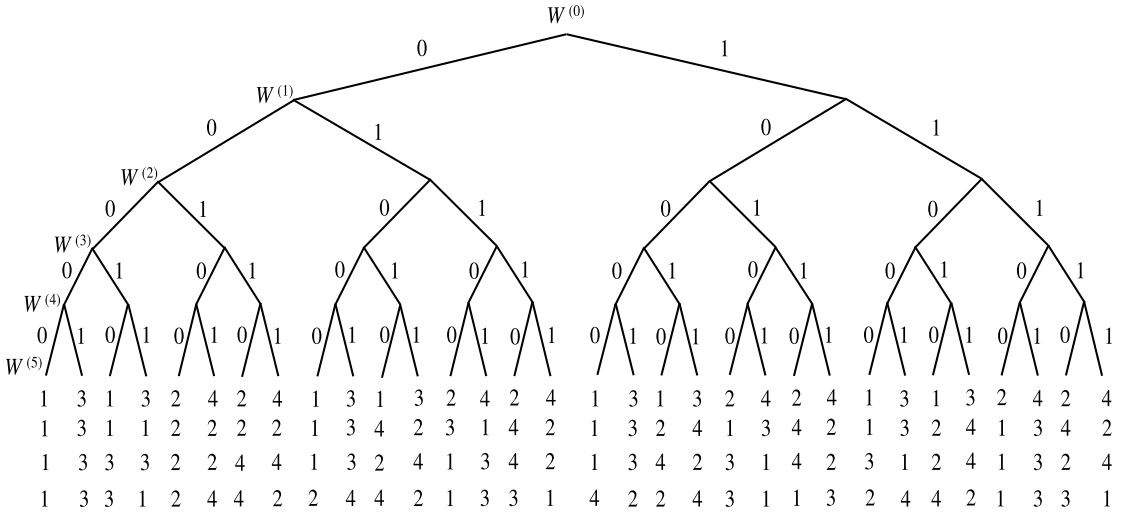

FIGURE 2. The five-level binary set partitioning tree.

Reed-Solomon code with the inner of the associated a multilevel high-rate space-time coding scheme based on the uniquely constructed five-level binary partition tree is also an original technique.

III. SET-PARTITIONING OF THE TRANSMISSION MATRIX

Orthogonal designs provide STBCs with full diversity and high transmission rate [15]. There are 256 of eight-dimensional signals in the 4 × QPSK signal set as shown in Figure 1. However, we only choose 32 out of the 256 signal points and construct the five-level partition tree to maintain the overall spectral efficiency at 2 bits/s/Hz.

It turns out that the five-level partition provides an optimal trade-off between spectral efficiency and complexity. If the number of partition is smaller than five, the spectral efficiency will be less than 2 bits/s/Hz due to the small number of outer codes. On the other hand, a larger number of partition will increase the complexity. Motivated by the proposed technique in [36], consider the orthogonal 2 × 2 code which is constructed by the following transmission matrix:

$$X = \begin{pmatrix} x_1 \sin\theta_1 - x_2^* \cos\theta_1 & x_3 \sin\theta_2 - x_4^* \cos\theta_2 \\ -x_3^* \sin\theta_2 + x_4 \cos\theta_2 & x_1^* \sin\theta_1 - x_2 \cos\theta_1 \end{pmatrix} \quad (1)$$

At the first time slot, the encoder transmits $x_1 \sin\theta_1 - x_2^* \cos\theta_1$ from antenna 1 and $x_3 \sin\theta_2 - x_4^* \cos\theta_2$ from antenna 2. At the second time slot, the encoder transmits $-x_3^* \sin\theta_2 + x_4 \cos\theta_2$ from antenna 1 and $x_1^* \sin\theta_1 - x_2 \cos\theta_1$ from antenna 2. 4 modulated signals x_1, x_2, x_3, x_4 are transmitted during 2 time slots. Therefore, the average rate is 2. Let $\mathbf{Y}$ denotes another transmission matrix. The optimal values for θ_1 and θ_2 are selected by the formula (2), which is an optimization problem that maximizes the coding gain with full diversity.

$$\{\theta_1, \theta_2\} = \underset{\theta_1+\theta_2=90^\circ}{arg\,max} \ \underset{\mathbf{X}\neq\mathbf{Y}}{min} \left| det(\mathbf{X} - \mathbf{Y}) \right| \quad (2)$$

Consider the QPSK signal set. It is derived in [36] that the optimal values of θ_1 and θ_2 are 63.4° and 26.6° respectively. Each eight-dimensional signal (x_1, x_2, x_3, x_4) is mapped into a transmission matrix. The minimum CGD parameter between two codewords is the ultimate goal of the STBC design to guarantee full diversity and increase the coding gain [37]. As shown in Figure 2, a unique five-level binary partition chain $P(5) = W^{(0)}/W^{(1)}/W^{(2)}/W^{(3)}/W^{(4)}/W^{(5)}$ is constructed through a computer exhausted search. Note that only 32 transmission matrices are included in $P(5)$.

The set-partitioning of of transmission matrix set is built under the CGD criterion, where the CGD between two matrices $\mathbf{X}$ and $\mathbf{Y}$ is defined as:

$$d(\mathbf{X}, \mathbf{Y}) = det\left[(\mathbf{X} - \mathbf{Y})(\mathbf{X} - \mathbf{Y})^H\right] \quad (3)$$

where det($\mathbf{X}$) is the determinant of the matrix $\mathbf{X}$.

For $1 \le p \le \lambda$, let the intraset CGD of $W^{(p)}$ be identified as:

$$\Delta^{(p)} = min\left\{d(\mathbf{X}, \mathbf{Y}) \middle| \mathbf{X}, \mathbf{Y} \in W^{(p-1)}, \mathbf{X} \neq \mathbf{Y}\right\} \quad (4)$$

It can be calculated that $\Delta^{(1)}$, $\Delta^{(2)}$, $\Delta^{(3)}$, $\Delta^{(4)}$, and $\Delta^{(5)}$ are 1.767, 1.767, 16, 16 and 64, respectively.

IV. THE MULTILEVEL CODING SCHEME

Consider a partition chain $P(\lambda) = W^{(0)}/W^{(1)}/\ldots/W^{(\lambda)}$, the λ-level concatenated scheme can be constructed as shown in Figure 3. For $1 \le p \le \lambda$, let $C^{(p)}$ denotes $(n, k^{(p)}, d^{(p)})$ binary linear block code, where n, $k^{(p)}$, and $d^{(p)}$ are the code length, dimension, and minimum Hamming distance, respectively. In the coded block

$$\begin{bmatrix} s_1^{(1)} & \ldots & s_n^{(1)} \\ \vdots & & \vdots \\ s_1^{(\lambda)} & \ldots & s_n^{(\lambda)} \end{bmatrix}$$

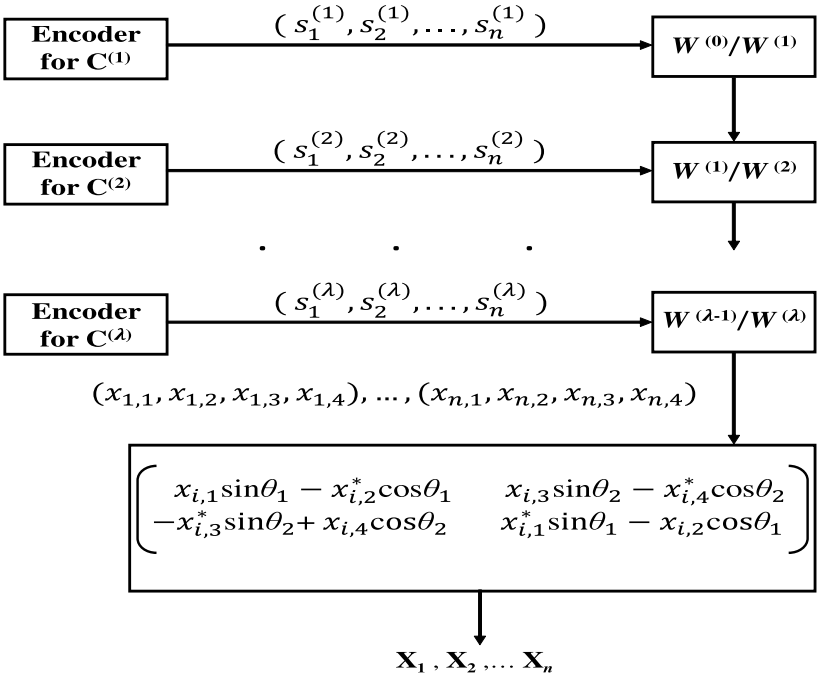

FIGURE 3. The encoding diagram of multilevel high-rate space-time block code (MHRSTBC).

each column vector

$$\begin{bmatrix} s_i^{(1)} \\ \vdots \\ s_i^{(\lambda)} \end{bmatrix}$$

corresponds to an eight-dimensional signal $(x_{i,1}, x_{i,2}, x_{i,3}, x_{i,4})$ for $1 \leq i \leq n$. These n signals are then mapped into n transmission matrices $\mathbf{X_1}, \mathbf{X_2}, \ldots, \mathbf{X_n}$. The symbols in the transmission matrices are transmitted during two time slots. The average spectral efficiency is defined as:

$$\frac{1}{2} \times \frac{\sum_{p=1}^{\lambda} k^{(p)}}{n} \; bits/s/Hz \tag{5}$$

The minimum CGD of the multilevel concatenated coding scheme is an important parameter for the error performance. The component codes $C^{(p)}$ are chosen so that the minimum CGD of each level is maximized. With a similar method derived in [38], the minimum CGD is expressed as:

$$\min_{1 \leq p \leq \lambda} \left\{ (d^{(p)})^2 \cdot \Delta^{(p)} \right\} \tag{6}$$

Example 1: Consider the partition chain $P^{(5)}$ in Figure 2. MHRSTBC-2 scheme can be designed by choosing $C^{(1)}, C^{(2)}, C^{(3)}, C^{(4)}, C^{(5)}$ as the (8,4,4), (8,4,4), (8,8,1), (8,8,1), and (8,8,1) binary linear block codes, respectively. From (5) and (6), the spectral efficiency and the minimum CGD of MHRSTBC-2 are 2 bits/s/Hz and 16, respectively. Please refer to Appendix A for a detailed listing of figures and tables used to further describe and explain the calculations of the spectral efficiency and the minimum CGD of MHRSTBC-2 in Example 1.

V. TWOFOLD CONCATENATION CODING SCHEME

Long codes can decrease the probability of error and it can help with both soft and hard decision decoding. Therefore, the concatenation method is used to construct long codes that can be decoded with less complexity [39], [40]. Multilevel concatenated codes with large minimum CGD can be designed easily by choosing appropriate binary block codes. However, there is a trade-off between the CGD and the decoding complexity. To design MHRSTBC with high CGD, the length of each component code must be large. Since the ML decoding of long block codes is computationally intensive with the modulation order, we adopt the concatenated coding technique to avoid large decoding complexity of long codes. Therefore, an outer RS code is concatenated with the inner multilevel coding scheme.

In this way, we can use short block codes as component codes of the inner multilevel coding scheme. The decoding complexity for ML of the inner short decoder is small. Moreover, the outer RS code is decoded by algebraic hard decoding. Hence, the proposed twofold concatenated scheme has long block length and reasonable decoding complexity. Figure 4 shows the coding structure of the twofold concatenated scheme.

In the outer encoding, the (N, K) RS code over GF (2^b) is interleaved by a depth of l. In the inner encoding, the spectral efficiency of the MHRSTBC scheme is $lb/2n$ bits/s/Hz. $K \times lb$ input bits

$$\begin{bmatrix} u_{1,1} & \cdots & u_{1,K} \\ \vdots & & \vdots \\ u_{lb,1} & \cdots & u_{lb,K} \end{bmatrix}$$

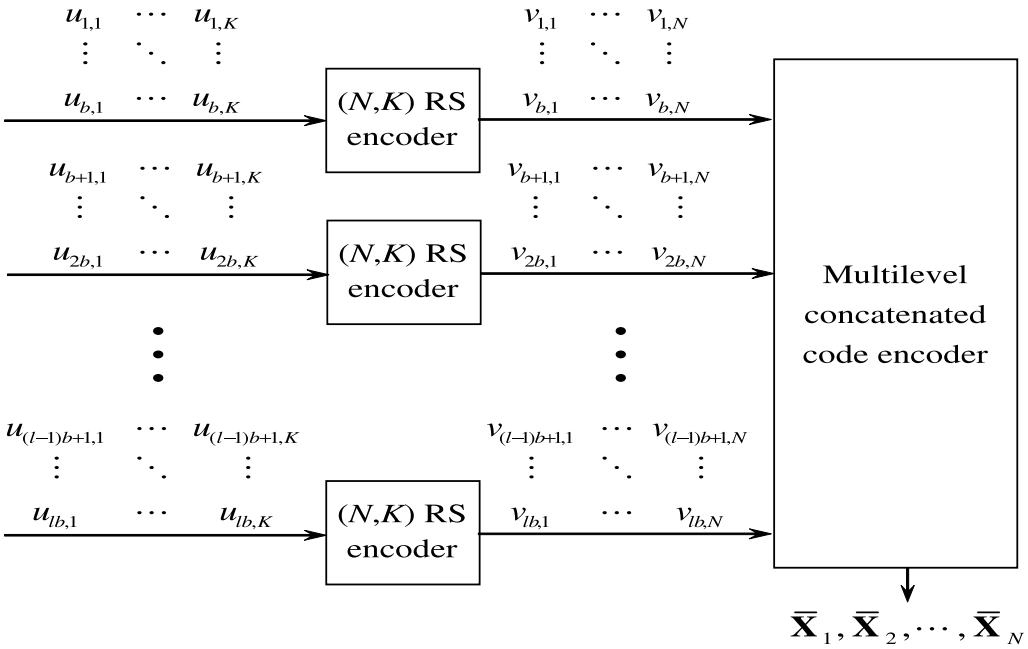

FIGURE 4. The coding architecture of the proposed twofold concatenated scheme.

are placed in an array of lb rows and K columns. In the outer code encoder, the K information symbols $(u_{(i-1)b+1,1}, \ldots u_{ib,1})^T, \ldots, (u_{(i-1)b+1,K}, \ldots u_{ib,K})^T$ are encoded into N coded symbols $(v_{(i-1)b+1,1}, \ldots, v_{ib,1})^T, \ldots, (v_{(i-1)b+1,N}, \ldots, v_{ib,N})^T$ for $1 \leq i \leq l$. In the inner code encoder, the lb bits $v_{1,j}, \ldots, v_{lb,j}$ are then encoded into the transmission matrix vector $\bar{X}_j = (x_{j,1}, x_{j,2}, \ldots, x_{j,n})$ for $1 \leq j \leq N$. The output sequence $\bar{X}_1, \bar{X}_2, \ldots, \bar{X}_N$ contains $N \times n$ transmission matrices. Therefore, the spectral efficiency is expressed as:

$$\frac{1}{2} \times \frac{K \times lb}{N \times n} \; bits/s/Hz \tag{7}$$

There are two steps in the decoding process. First, the inner code is decoded by using the multistage decoding. The squared Euclidean distance is used as the metric in the Viterbi soft decoding algorithm. Second, for $1 \leq i \leq l$, the symbols $(\hat{v}_{(i-1)b+1,1}, \ldots, \hat{v}_{ib,1})^T, \ldots, (\hat{v}_{(i-1)b+1,N}, \ldots, \hat{v}_{ib,N})^T$ are applied at the input of the RS algebraic hard decoder.

Example 2: Consider the five-level partition chain $P(5)$ in Figure 2. Let the five component codes of the MHRSTBC-2 be the (10,9,2), (10,9,2), (10,10,1), (10,10,1), and (10,10,1) binary block codes, respectively. A twofold RS-MHRSTBC scheme can be designed for which (255,213) RS code is the outer code and MHRSTBC-2 is the inner code. The interleaving depth of the outer code is $l = 6$. The spectral efficiency of RS-MHRSTBC-2 is 2 bit/s/Hz. Please refer to Appendix B for a more detailed explanation of Example 2.

VI. SIMULATION RESULTS

The bit error rate (BER) curve is used to evaluate the performance quality of the proposed scheme, where the y-axis represents the average BER, and the x-axis represents the ratio of signal energy per symbol to noise power density per hertz (E_s/N_0), it is also known as the signal to noise ratio (SNR). Table 1 shows the main parameters used in the simulation. Figure 5 shows the performance comparison between the proposed scheme and other schemes by plotting the BER against the E_s/N_0 (dB) using two transmit antennas and two receive antennas over AWGN and Rayleigh flat-fading channels. It is observed that our proposed RS-MHRSTBC can achieve significant coding gains. From Figure 5, it can also be seen that RS-MHRSTBC outperforms the other coding schemes at medium SNR. Table 2 shows the significant performance enhancement in the coding gain of the proposed coding scheme RS-MHRSTBC as compared to the other schemes. In addition, since the RS code uses the algebraic hard decoding, the decoding complexity is very small compared with the soft decoding. However, the block length of the multilevel block codes to which the Viterbi soft decoding was applied, is short and the trellis complexity is rather low. The trellis complexity of the block code (8,4,4) and (8,8,1) is

TABLE 1. The main simulation parameters.

Parameters	Settings
Code Length	2550
Spectral Efficiency	2.0
Modulator	QPSK
Number of MIMO Antennas	2×2
Channel	AWGN & Flat Rayleigh-Fading

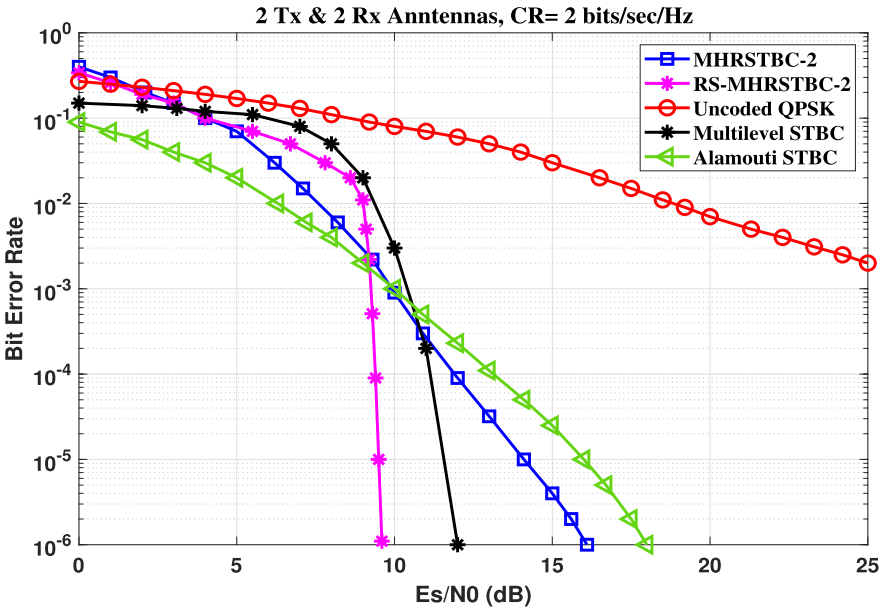

FIGURE 5. BER Vs Es/N0 of the proposed RS-MHRSTBC-2 and different schemes using 2 × 2 antennas with spectral efficiency (SE) of 2 bits/s/Hz over AWGN and flat Rayleigh fading channels.

TABLE 2. Coding gains over uncoded QPSK.

BER	10^{-3}	10^{-4}	10^{-5}	10^{-6}
Alamouti STBC [15]	16.75 dB	22.28 dB	30.55 dB	38.12 dB
MHRSTBC-2	**17.05 dB**	**24.11 dB**	**32.41 dB**	**40.17 dB**
Multilevel STBC [19]	16.58 dB	24.86 dB	34.91 dB	44.30 dB
RS-MHRSTBC-2	**18.58 dB**	**27.38 dB**	**37.75 dB**	**47.79 dB**

TABLE 3. List of codewords for the linear block code (8,4,4).

Number	Message words	16-Codeword
1	0000	00000000
2	0001	11111111
3	0010	11110000
4	0011	00001111
5	0100	01010101
6	0101	10101010
7	0110	10100101
8	0111	01011010
9	1000	00110011
10	1001	11001100
11	1010	11000011
12	1011	00111100
13	1100	01100110
14	1101	10011001
15	1110	10010110
16	1111	01101001

35 and 8 respectively. On the other hand, the trellis complexity of the block code (10,9,2) and (10,10,1) is 53 and 10 respectively, where trellis complexity refers to the number of additions and comparisons. Therefore, in comparison to Alamouti STBC and Multilevel STBC, our proposed scheme can achieve large coding gain with a little higher decoding complexity.

VII. CONCLUSION AND FUTURE WORK

We proposed a channel coding scheme architecture that can meet the efficiency and reliability requirements in IoTs over MIMO-based WMNs and boosts various promising IoTs applications without compromising diversity and spectral efficiency. The RS-MHRSTBC design offered significant coding gains enhancement in WMNs over Rayleigh fading and AWGN channels. Moreover, the inner soft-decision and outer hard-decision decoding algorithm has given the proposed scheme a reasonable decoding complexity. The proposed scheme was evaluated by the BER and E_s/N_0 metrics using two transmit antennas and two receive antennas over a Rayleigh flat-fading and AWGN channel with a spectral efficiency of 2 bits/sec/Hz. Our proposed RS-MHRSTBC outperformed Alamouti STBC and Multilevel STBC in terms of coding gain over uncoded QPSK at the same bit error rate levels, 10^{-3}, 10^{-4}, 10^{-5}, 10^{-6}, where RS-MHRSTBC reached 18.58 dB, 27.38 dB, 37.75 dB, and 47.79 dB, respectively. While the proposed RS-MHRSTBC shows promising performance as compared to the classic Alamouti STBC and Multilevel STBC, our future work will explore the combinations of the MHRSTBC with more recent Turbo code, LDPC or Polar code to study their trade-off between energy efficiency and coding gains for wireless networks.

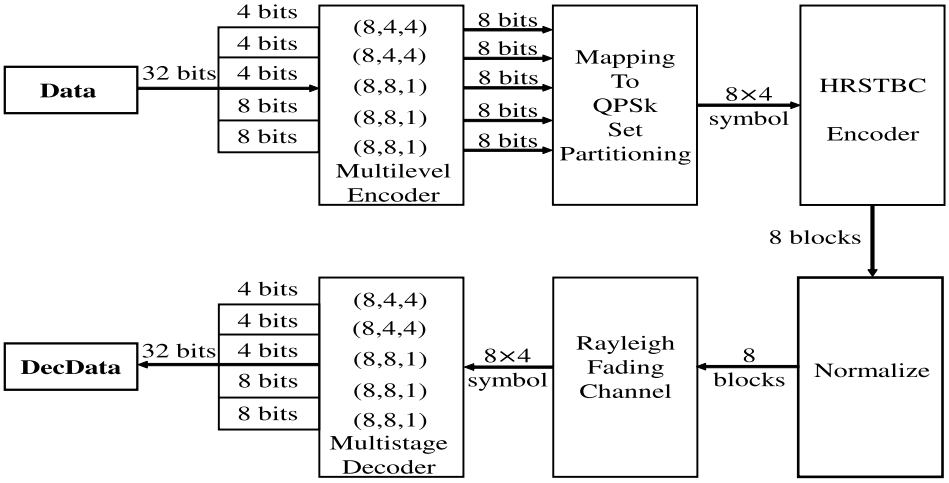

FIGURE 6. The block diagram of MHRSTBC-2 architecture.

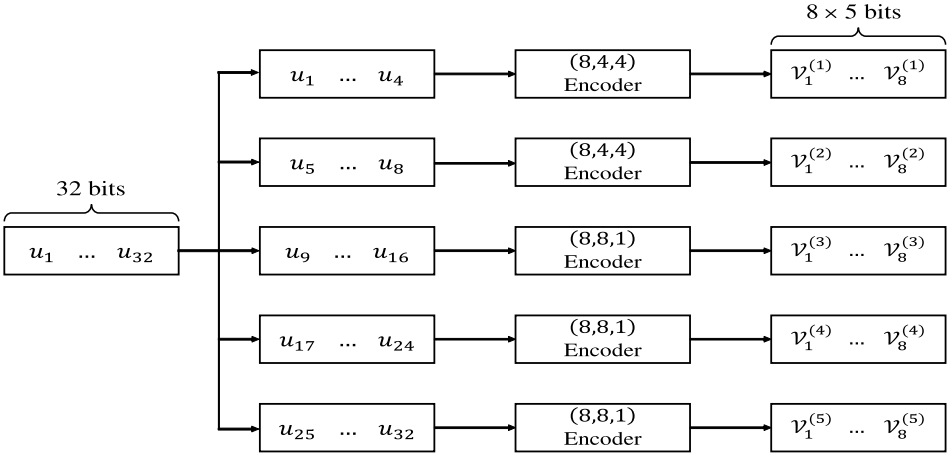

FIGURE 7. The MHRSTBC-2 encoding architecture diagram.

APPENDIX A

Example 1: As shown in Figure 6, we use two sets of (8,4,4) codes and three sets of (8,8,1) codes, and combine them with a five-level modulator set partitioning. In the encoding process of the MHRSTBC-2, each bit is mapped to the signal sequence $\{s_1, s_2, s_3, s_4\}$ and then transmitted through the transmitting antenna after being encoded by HRSTBC. The eight transmission matrices pass through the Rayleigh fading channel and add AWGN noise to simulate various interference the signal may encounter. At the receiving end, the received message symbols are decoded according to the trellis to which each level belongs.

The encoding process starts with generating a set of 32 bits of the original signal $u = (u_1, u_2, \dots, u_{32})$. $u_1, \dots, u_4$ and $u_5, \dots, u_8$ are encoded into (8,4,4) using Reed-Muller encoding as shown in Figure 7. Table 3 represents the 16 codewords of the linear code (8,4,4). The generator matrix δ_{m1} for this example is shown below:

$$\delta_{m1} = \begin{bmatrix} 0 & 0 & 1 & 1 & 0 & 0 & 1 & 1 \\ 0 & 1 & 0 & 1 & 0 & 1 & 0 & 1 \\ 1 & 1 & 1 & 1 & 0 & 0 & 0 & 0 \\ 1 & 1 & 1 & 1 & 1 & 1 & 1 & 1 \end{bmatrix}$$

As shown in Figure 8, every code segment of five bits $v_i^{(1)}, v_i^{(2)}, v_i^{(3)}, v_i^{(4)}, v_i^{(5)}$, $i = 1, 2, \dots, 8$, is encoded and mapped into the QPSK set partitioning chain (32 branches in total). The signal sequence $s_{1,i}, s_{2,i}, s_{3,i}, s_{4,i}$, $i = 1, 2, \dots, 8$ is encoded by the high-rate space time block code, and then the transmission energy is normalized and transmitted. 32 branches of codewords $\{00000, 00001, \dots, 11110, 11111\}$ are mapped to the corresponding branches of the set split chain.

As shown in Table 4, from (5) and (6), the spectral efficiency and the minimum CGD of MHRSTBC-2 for each level

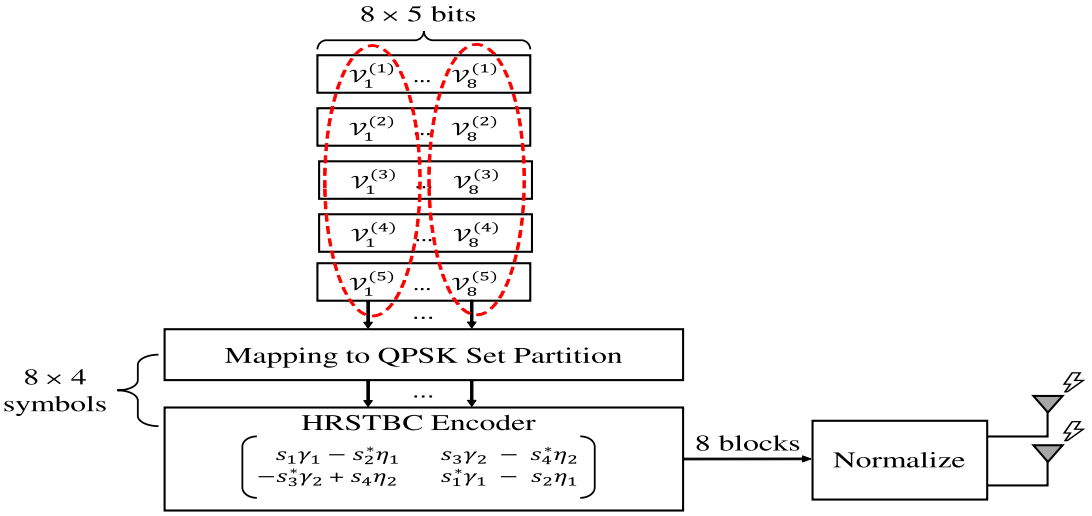

FIGURE 8. The MHRSTBC-2 message transmission architecture.

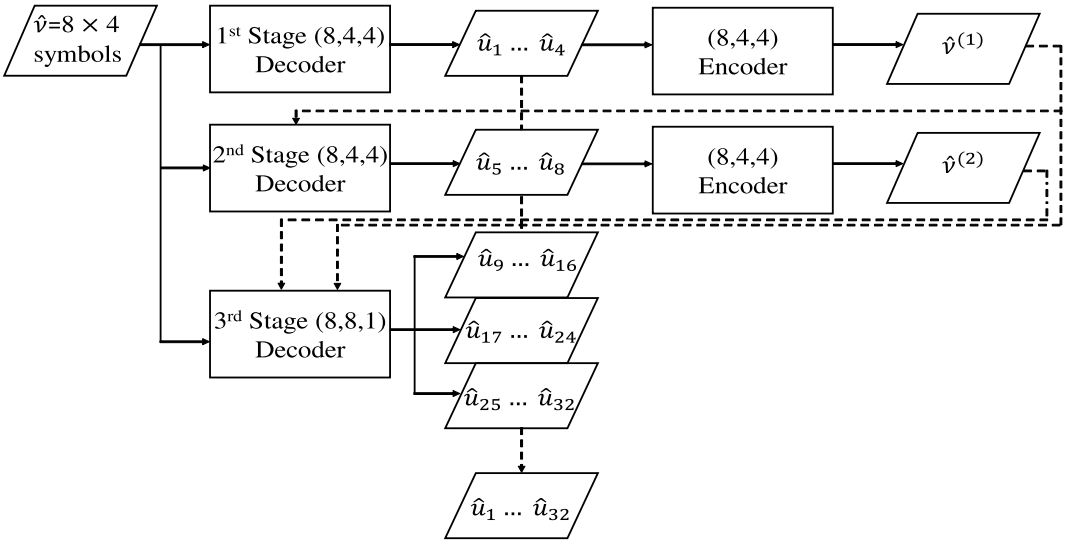

FIGURE 9. The five-level MHRSTBC-2 decoding architecture.

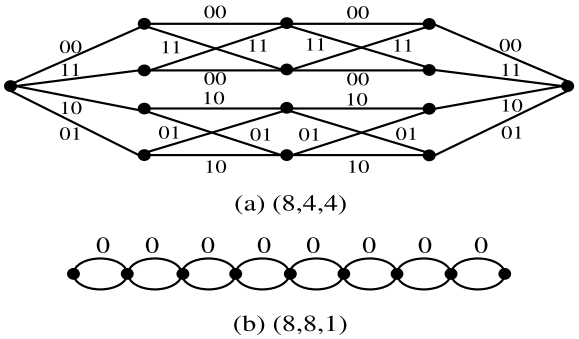

FIGURE 10. The MHRSTBC-2 decoding trellis of (8,4,4), (8,8,1).

can be calculated as:

$$(d^{(p)^2}) \cdot \Delta^{(p)} = \{(4^{(1)})^2 \times 1.767, (4^{(2)})^2 \times 1.767, (1^{(3)})^2 \times 16, (1^{(4)})^2 \times 16, (1^{(5)})^2 \times 64,\ 1 \le p \le 5\}.$$

$$min\{CGD((d^{(p)^2}) \times \Delta^{(p)})\} = min((28.272, 28.272, 16, 16, 6) = 16,\ 1 \le p \le 5.$$

Spectral efficiency (SE) is

$$SE = \frac{32}{2 \times 16} = 2\ bits/s/Hz.$$

Figure 9 shows the received signal $\hat{v}$ enters to the first stage (8, 4, 4) decoder, and the shortest path is calculated through the corresponding trellis and soft decision decoding. The data bits $\hat{u}_1 \ldots \hat{u}_4$ are extracted and re-encoded using the (8,4,4) encoder to obtain the codeword $\hat{v}^{(1)}$. In the second stage of the decoding process, the received signal $\hat{v}$ and the previously decoded codeword $\hat{v}^{(1)}$ are sent to the second stage (8, 4, 4) decoder through the associated trellis and the soft decision decoding to calculate the shortest path. The data bits $\hat{u}_5 \ldots \hat{u}_8$ are extracted and re-encoded by the (8, 4, 4) encoder to obtain the codeword $\hat{v}^{(2)}$. In the third level decoding process,

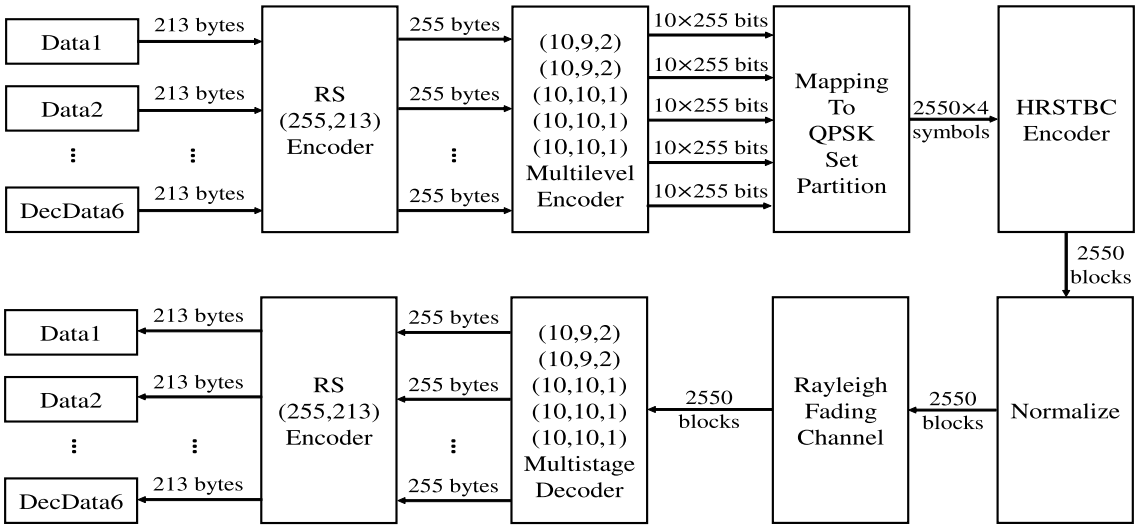

FIGURE 11. The overall RS-MHRSTBC-2 architecture diagram.

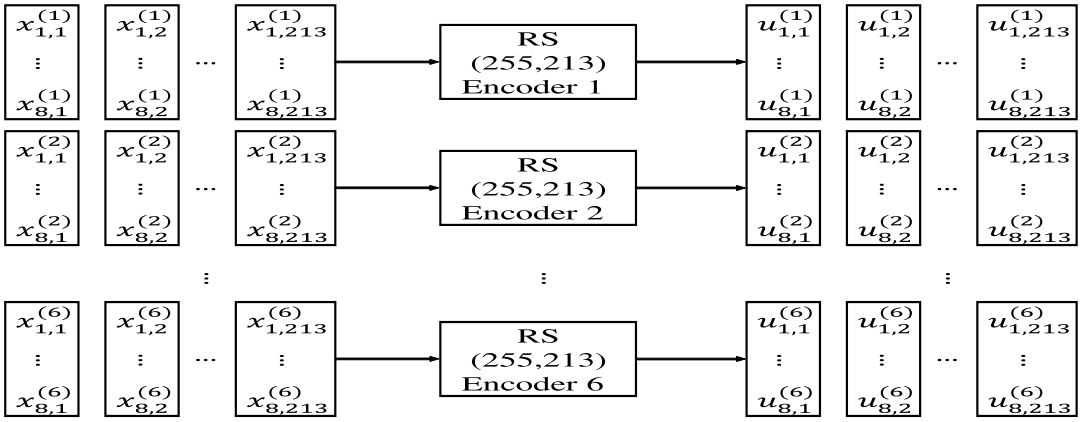

FIGURE 12. The RS-MHRSTBC-2 with the outer RS coding architecture diagram.

TABLE 4. The minimum hamming distance, inner-CGD, and CGD for every level of the binary partition chain.

Level	Minimum Hamming Distance (d)	Intraset CGD ($\triangle$)	CGD
1	4	1.767	28.272
2	4	1.767	28.272
3	1	16	16
4	1	16	16
5	1	64	64

the received signal $\hat{v}$ and the previously decoded codewords $\hat{v}^{(1)}$, $\hat{v}^{(2)}$ are sent to the third stage (8, 8, 1) decoder. The decoder calculates the shortest path through the associated trellis and soft decision decoding, and simultaneously extract the data bits $\hat{u}_9 \ldots \hat{u}_{16}, \hat{u}_{17} \ldots \hat{u}_{24}, \hat{u}_{25} \ldots \hat{u}_{32}$ of the third, fourth, and fifth level. Finally, the data bits extracted from each level are combined into a sequence of data bits to form a corrected restored signal. The trellis diagram of linear block decoder at each level is shown in Figure 10.

APPENDIX B

Example 2: As shown in Figure 11, the RS-MHRSTBC-2 is constructed by concatenating Reed-Solomon codes with the multilevel block codes. The outer RS (N, K, t) is encoded as six RS data blocks (255, 213), with error correction capability $t = (n - k)/2 = 21$ symbols, indicating that the message symbol has a length of 213 and the encoded codeword has a length of 255. First, we generated six sets of the original signal of 213 bytes, through RS (255,227) code to obtain 255 bytes as shown in Figure 12. Figure 13 illustrates the six groups of signals that are organized in parallel and vertical order. Each row of 48 bits corresponds

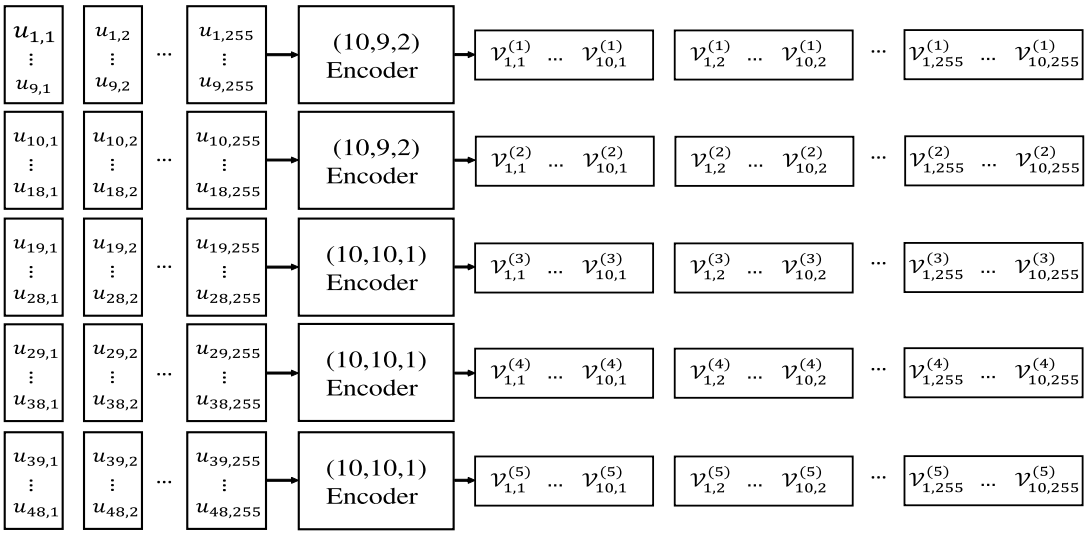

FIGURE 13. RS-MHRSTBC-2 coding architecture diagram.

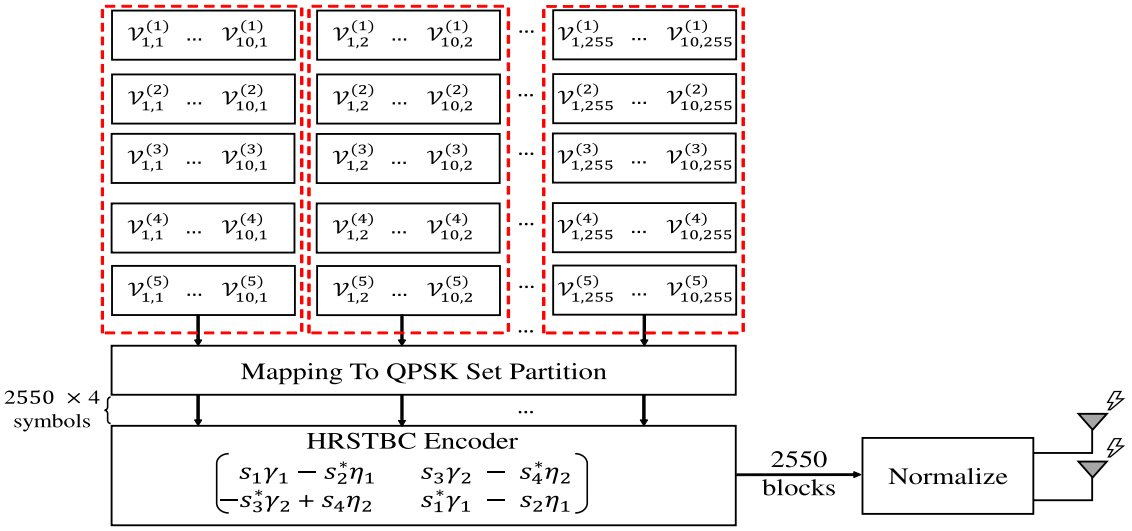

FIGURE 14. RS-MHRSTBC-2 transmission architecture.

to two groups of (10, 9, 2) and three groups of (10, 10, 1) codes. The data bits $u_1 \ldots u_9$ are encoded into the (10, 9, 2) encoder for even parity encoding to get the first level of the codewords $v_{1,i}^{(1)}, v_{2,i}^{(1)}, \ldots, v_{10,i}^{(1)}$, $i = 1, 2, \ldots, 255$. $u_{10} \ldots u_{18}$ are encoded into the (10,9,2) encoder for even parity encoding to get the second level of the codewords $v_{1,i}^{(2)}, v_{2,i}^{(2)}, \ldots, v_{10,i}^{(2)}$, $i = 1, 2, \ldots, 255$. $u_{19} \ldots u_{28}$ are encoded into the (10,10,1) encoder without encoding to get the third level of the codewords $v_{1,i}^{(3)}, v_{2,i}^{(3)}, \ldots, v_{10,i}^{(3)}$, $i = 1, 2, \ldots, 255$. The coding methods for the fourth and fifth levels are the same as the third level.

As shown in Figure 14, block coding signals $\left\{v_{i,j}^{(1)}, v_{i,j}^{(2)}, v_{i,j}^{(3)}, i = 1, 2, \ldots, 8, j = 1, 2, \ldots, 255\right\}$ are encoded and each row of codewords is mapped into the QPSK set partitioning chain (32 branches in total). Next, $s_{1,i}, s_{2,i}, s_{3,i}, s_{4,i}$, $i = 1, 2, \ldots, 10$ are encoded by the high-rate space time block code, and then transmitted after normalizing the transmission energy. 32 kind of signals $\{00000, 00001, \ldots, 11110, 11111\}$ are mapped to the corresponding branches of the collection segmentation chain, and transmitted at the same time after being encoded by high-rate space-time code and the transmission energy is normalized.

The signal segments $v_{i,j}^{(1)}$, $v_{i,j}^{(2)}$, $v_{i,j}^{(3)}$, $i = 1, 2, \ldots, 255$ are encoded and each row of codewords is mapped to the QPSK set partitioning. The binary linear block codes $C^{(1)}, C^{(2)}, C^{(3)}, C^{(4)}, C^{(5)}$ are (10,9,2), (10,9,2), (10,10,1), (10,10,1), (10,10,1) respectively. Based on Table 5, the spectral efficiency and the minimum CGD of MHRSTBC-2 of

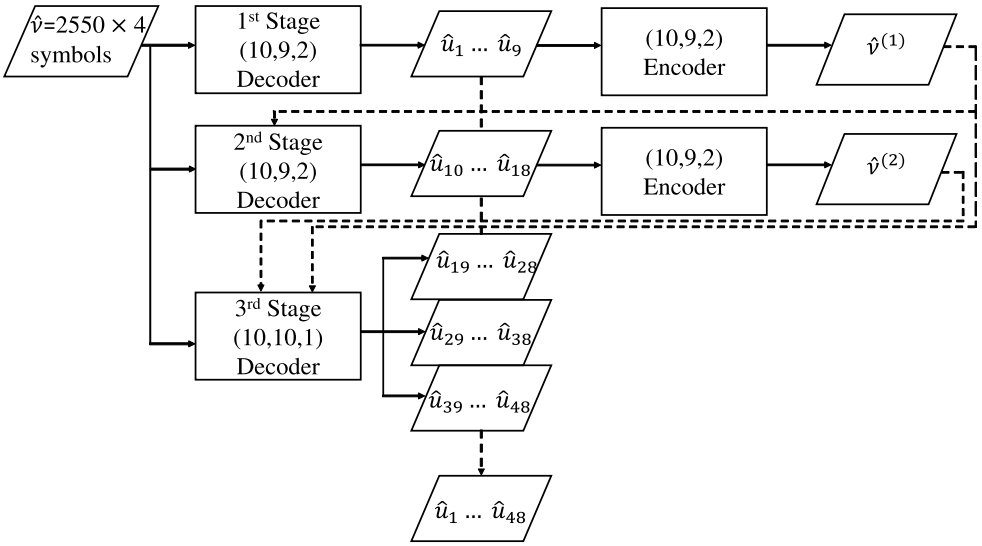

FIGURE 15. The decoding architecture of the RS-MHRSTBC-2.

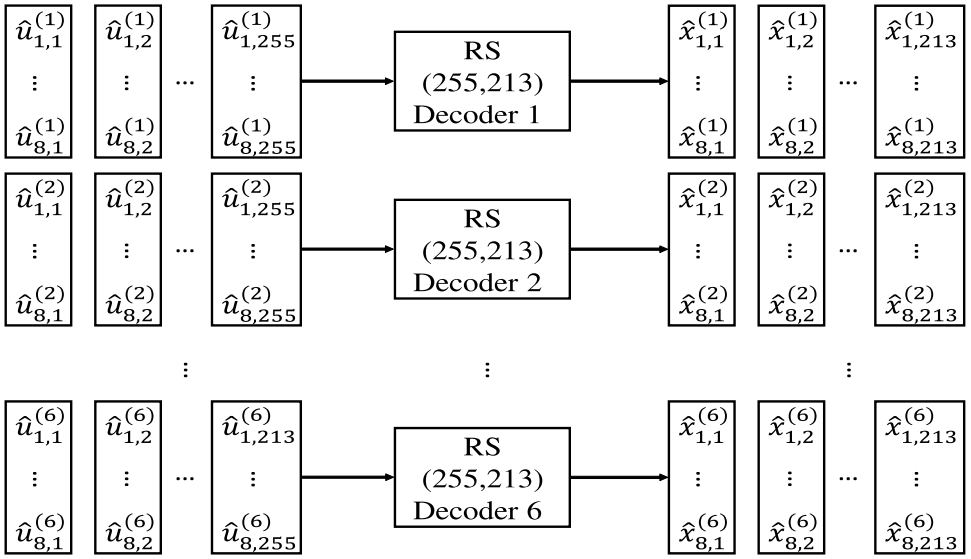

FIGURE 16. The RS-MHRSTBC-2 with the outer RS decoding architecture diagram.

TABLE 5. The minimum hamming distance, inner-CGD, and CGD for every level of the binary partition chain.

Level	Minimum Hamming Distance (d)	Intraset CGD (Δ)	CGD
1	2	1.767	7.068
2	2	1.767	7.068
3	1	16	16
4	1	16	16
5	1	64	64

each level can be calculated as:

$$(d^{(p)^2}) \cdot \Delta^{(p)} = \left\{(2^{(1)})^2 \times 1.767, (2^{(2)})^2 \times 1.767, (1^{(3)})^2 \times 16, (1^{(4)})^2 \times 16, (1^{(5)})^2 \times 64,\ 1 \le p \le 5\right\}.$$

$$min\left\{CGD((d^{(p)^2}) \times \Delta^{(p)})\right\} = min((7.068, 7.068, 16, 16, 64) = 7.068,\ 1 \le p \le 5.$$

Spectral efficiency (SE) is

$$SE = \frac{213}{255} \times \frac{48}{20} = \frac{10244}{5100} \cong 2\ bits/s/Hz.$$

As shown in Figure 15, the received signal $\hat{v}$ is decoded by the first stage (10,9,2) decoder, and the shortest path is calculated through the corresponding trellis graph and soft decision decoding. The data bits $\hat{u}_1 \ldots \hat{u}_9$ are extracted and re-encoded using the (10,9,2) encoder to obtain the codeword $\hat{v}^{(1)}$. In the second stage of the decoding process, the received signal $\hat{v}$ and the previously decoded codeword $\hat{v}^{(1)}$ are sent to the second stage (10, 9, 2) decoder through the associated trellis and the soft decision decoding to calculate the shortest path.

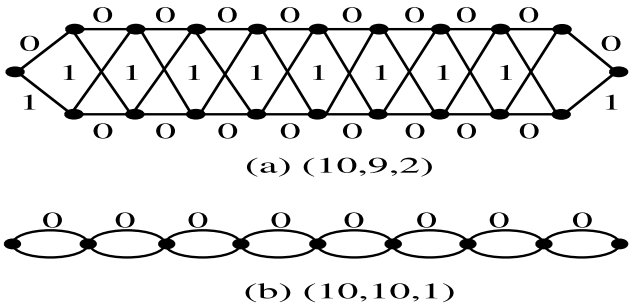

FIGURE 17. The RS-MHRSTBC-2 decoding trellis of (10,9,2), (10,10,1).

The data bits $\hat{u}_5 \ldots \hat{u}_8$ are extracted and re-encoded by the (10, 9, 2) encoder to obtain the codeword $\hat{v}^{(2)}$. In the third level decoding process, the received signal $\hat{v}$ and the previously decoded codewords $\hat{v}^{(1)}$, $\hat{v}^{(2)}$ are sent to the third stage (10, 10, 1) decoder. The decoder calculates the shortest path through the associated trellis and soft decision decoding, and simultaneously extract the data bits $\hat{u}_{19} \ldots \hat{u}_{28}$, $\hat{u}_{29} \ldots \hat{u}_{38}$, $\hat{u}_{39} \ldots \hat{u}_{48}$ of the third, fourth, and fifth level. Finally, the data bits extracted from each level are combined into a sequence of data bits to form a corrected restored signal. The trellis diagram of the linear block decoder (10,9,2) and (10,10,1) is shown in Figure 17.

REFERENCES

[1] Y. Liu, K.-F. Tong, X. Qiu, Y. Liu, and X. Ding, "Wireless mesh networks in IoT networks," in *Proc. Int. Workshop Electromagn., Appl. Student Innov. Competition*, Jun. 2017, pp. 183–185.

[2] A. Zanella, N. Bui, A. Castellani, L. Vangelista, and M. Zorzi, "Internet of Things for smart cities," *IEEE Internet Things J.*, vol. 1, no. 1, pp. 22–32, Feb. 2014.

[3] L. Catarinucci, D. de Donno, L. Mainetti, L. Palano, L. Patrono, M. L. Stefanizzi, and L. Tarricone, "An IoT-aware architecture for smart healthcare systems," *IEEE Internet Things J.*, vol. 2, no. 6, pp. 515–526, Dec. 2015.

[4] M. Chiang and T. Zhang, "Fog and IoT: An overview of research opportunities," *IEEE Internet Things J.*, vol. 3, no. 6, pp. 854–864, Dec. 2016.

[5] I. F. Akyildiz, X. Wang, and W. Wang, "Wireless mesh networks: A survey," *Comput. Netw.*, vol. 47, no. 4, pp. 445–487, Mar. 2005.

[6] D. Chew, *The Wireless Internet Things: A Guide to Lower Layers*. Hoboken, NJ, USA: Wiley, 2018.

[7] R. Bruno, M. Conti, and E. Gregori, "Mesh networks: Commodity multihop ad hoc networks," *IEEE Commun. Mag.*, vol. 43, no. 3, pp. 123–131, Mar. 2005.

[8] Cisco. *Cisco Annual Internet Report White Paper, 2018–2023*. Accessed: Mar. 24, 2020. [Online]. Available: https://www.cisco.com/c/en/us/index.html

[9] A. Al-Fuqaha, M. Guizani, M. Mohammadi, M. Aledhari, and M. Ayyash, "Internet of Things: A survey on enabling technologies, protocols, and applications," *IEEE Commun. Surveys Tuts.*, vol. 17, no. 4, pp. 2347–2376, 4th Quart., 2015.

[10] J. Lin, W. Yu, N. Zhang, X. Yang, H. Zhang, and W. Zhao, "A survey on Internet of Things: Architecture, enabling technologies, security and privacy, and applications," *IEEE Internet Things J.*, vol. 4, no. 5, pp. 1125–1142, Oct. 2017.

[11] I. F. Akyildiz and X. Wang, "A survey on wireless mesh networks," *IEEE Commun. Mag.*, vol. 43, no. 9, pp. S23–S30, Sep. 2005.

[12] C. Xu, S. Sugiura, S. X. Ng, P. Zhang, L. Wang, and L. Hanzo, "Two decades of MIMO design tradeoffs and reduced-complexity MIMO detection in near-capacity systems," *IEEE Access*, vol. 5, pp. 18564–18632, 2017.

[13] A. F. Naguib, V. Tarokh, N. Seshadri, and A. R. Calderbank, "A space-time coding modem for high-data-rate wireless communications," *IEEE J. Sel. Areas Commun.*, vol. 16, no. 8, pp. 1459–1478, Oct. 1998.

[14] V. Tarokh, A. Naguib, N. Seshadri, and A. R. Calderbank, "Space-time codes for high data rate wireless communication: Performance criteria in the presence of channel estimation errors, mobility, and multiple paths," *IEEE Trans. Commun.*, vol. 47, no. 2, pp. 199–207, Feb. 1999.

[15] S. M. Alamouti, "A simple transmit diversity technique for wireless communications," *IEEE J. Sel. Areas Commun.*, vol. 16, no. 8, pp. 1451–1458, Oct. 1998.

[16] V. Tarokh, H. Jafarkhani, and A. R. Calderbank, "Space-time block codes from orthogonal designs," *IEEE Trans. Inf. Theory*, vol. 45, no. 5, pp. 1456–1467, Jul. 1999.

[17] Z. Chen, J. Yuan, B. Vucetic, and Z. Zhou, "Performance of Alamouti scheme with transmit antenna selection," *Electron. Lett.*, vol. 39, no. 23, pp. 1666–1668, Nov. 2003.

[18] V. Tarokh, N. Seshadri, and A. R. Calderbank, "Space-time codes for high data rate wireless communication: Performance criterion and code construction," *IEEE Trans. Inf. Theory*, vol. 44, no. 2, pp. 744–765, Mar. 1998.

[19] D.-F. Yuan, P. Zhang, and Q. Wang, "Multilevel codes (MLC) with multiple antennas over Rayleigh fading channels," in *Proc. IEEE 54th Veh. Technol. Conf. VTC Fall*, Oct. 2001, pp. 1289–1293.

[20] Y. Yan, B. Zhang, H. T. Mouftah, and J. Ma, "Practical coding-aware mechanism for opportunistic routing in wireless mesh networks," in *Proc. IEEE Int. Conf. Commun.*, 2008, pp. 2871–2876.

[21] S. Katti, H. Rahul, W. Hu, D. Katabi, M. Médard, and J. Crowcroft, "XORs in the air: Practical wireless network coding," in *Proc. Conf. Appl., Technol., Archit., Protocols Comput. Commun.*, Aug. 2006, pp. 243–254.

[22] Y. Yan, B. Zhang, J. Zheng, and J. Ma, "CORE: A coding-aware opportunistic routing mechanism for wireless mesh networks [accepted from open call," *IEEE Wireless Commun.*, vol. 17, no. 3, pp. 96–103, Jun. 2010.

[23] Y. Fang, P. Chen, G. Cai, F. C. M. Lau, S. C. Liew, and G. Han, "Outage-limit-approaching channel coding for future wireless communications: Root-protograph low-density parity-check codes," *IEEE Veh. Technol. Mag.*, vol. 14, no. 2, pp. 85–93, Jun. 2019.

[24] P. Chen, Z. Xie, Y. Fang, Z. Chen, S. Mumtaz, and J. J. P. C. Rodrigues, "Physical-layer network coding: An efficient technique for wireless communications," *IEEE Netw.*, vol. 34, no. 2, pp. 270–276, Mar. 2020.

[25] Y. Fang, G. Han, G. Cai, F. C. M. Lau, P. Chen, and Y. L. Guan, "Design guidelines of low-density parity-check codes for magnetic recording systems," *IEEE Commun. Surveys Tuts.*, vol. 20, no. 2, pp. 1574–1606, Sec. 2018.

[26] E. Arikan, "Channel polarization: A method for constructing capacity-achieving codes for symmetric binary-input memoryless channels," *IEEE Trans. Inf. Theory*, vol. 55, no. 7, pp. 3051–3073, Jul. 2009.

[27] C. Berrou and A. Glavieux, "Near optimum error correcting coding and decoding: Turbo-codes," *IEEE Trans. Commun.*, vol. 44, no. 10, pp. 1261–1271, Oct. 1996.

[28] Z. H. Kashani and M. Shiva, "BCH coding and multi-hop communication in wireless sensor networks," in *Proc. IFIP Int. Conf. Wireless Opt. Commun. Netw.*, Apr. 2006, p. 5.

[29] R. G. Gallager, "Low-density parity-check codes," *IRE Trans. Inf. Theory*, vol. IT-8, no. 1, pp. 21–28, Jan. 1962.

[30] I. S. Reed and G. Solomon, "Polynomial codes over certain finite fields," *J. Soc. Ind. Appl. Math.*, vol. 8, no. 2, pp. 300–304, Jun. 1960.

[31] L. Biard and D. Noguet, "Choice and implementation of a Reed–Solomon code for low power low data rate communication systems," in *Proc. IEEE Radio Wireless Symp.*, Jan. 2007, pp. 365–368.

[32] C. Desset and A. Fort, "Selection of channel coding for low-power wireless systems," in *Proc. 57th IEEE Semiannu. Veh. Technol. Conf. VTC-Spring.*, Apr. 2003, pp. 1920–1924.

[33] L. Song, K. K. Parhi, I. Kuroda, and T. Nishitani, "Hardware/software codesign of finite field datapath for low-energy Reed–Solomon codecs," *IEEE Trans. Very Large Scale Integr. (VLSI) Syst.*, vol. 8, no. 2, pp. 160–172, Apr. 2000.

[34] P. Lettieri, C. Fragouli, and M. B. Srivastava, "Low power error control for wireless links," in *Proc. 3rd Annu. ACM/IEEE Int. Conf. Mobile Comput. Netw. MobiCom*, 1997, pp. 139–150.

[35] S. B. Wicker, "Reed–Solomon error control coding for Rayleigh fading channels with feedback," *IEEE Trans. Veh. Technol.*, vol. 41, no. 2, pp. 124–133, May 1992.

[36] V. Vakilian and H. Mehrpouyan, "High-rate and low-complexity space-time block codes for 2 × 2 mimo systems," *IEEE Commun. Lett.*, vol. 20, no. 6, pp. 1227–1230, Jun. 2016.

[37] H. Jafarkhani and N. Seshadri, "Super-orthogonal space-time trellis codes," *IEEE Trans. Inf. Theory*, vol. 49, no. 4, pp. 937–950, Apr. 2003.
[38] S.-C. Ma and C.-H. Lin, "Multilevel concatenated space-time block codes," in *Proc. Int. Conf. Syst. Sci. Eng.*, Jul. 2010, pp. 349–351.
[39] M. Tomlinson, C. J. Tjhai, M. A. Ambroze, M. Ahmed, and M. Jibril, *Error-Correction Coding and Decoding*. Cham, Switzerland: Springer, 2017, p. 522.
[40] C. Xing, H. Niederreiter, and K. Yan Lam, "A generalization of algebraic-geometry codes," *IEEE Trans. Inf. Theory*, vol. 45, no. 7, pp. 2498–2501, Nov. 1999.

SHANG-CHIH MA (Member, IEEE) received the Ph.D. degree in electrical engineering from National Taiwan University, Taipei City, Taiwan, in 1994. He is currently an Associate Professor with the Department of Electrical Engineering, National Taipei University of Technology. His current research interests include, signal processing, wireless sensor networks, information theory, digital communication systems, the IoTs, and channel coding.

MOHAMMAD ALKHALEEFAH (Member, IEEE) is currently pursuing the Ph.D. degree with the Electrical Engineering and Computer Science (EECS), Electrical Engineering Department, National Taipei University of Technology, Taipei City, Taiwan. His research interests include information theory, deep learning, image processing, data science, pattern recognition, computer vision, remote sensing, and the IoTs.

YANG-LANG CHANG (Senior Member, IEEE) received the Ph.D. degree in computer science and information engineering from National Central University, Taiwan, in 2003. He started his career with NDC IBM Taiwan as a Hardware Design Engineer before joining ALCATEL as a Software Development Engineer. He was a Visiting Scientist with the Space Science and Engineering Center, University of Wisconsin–Madison. He is currently a Professor and the Chair of the Electrical Engineering Department, National Taipei University of Technology. He is also the Director of the High Performance Computing and Deep Learning Laboratory and the NVIDIA-Taipei Tech Embedded GPU Joint Laboratory, National Taipei University of Technology. His research interests include remote sensing, high performance computing, deep learning, pattern recognition, and image processing. He is also the Chair of Taipei Chapter of IEEE Geoscience and Remote Sensing Society.

LENA CHANG (Member, IEEE) received the Ph.D. degree in electrical engineering from National Taiwan University, in 1992. From 1987 to 1988, she worked as an Electrical Engineer with the Department of Research and Development, ADI Corporation, Taipei City. From 1992 to 2003, she was an Associate Professor with the Department of Merchant Marine, National Taiwan Ocean University. Since 2003, she has been an Associate Professor with the Department of Communications, Navigation and Control Engineering, National Taiwan Ocean University. Her research interests are in the areas of remote sensing, adaptive arrays, adaptive signal processing, and image processing. She is a member of the Phi Tau Phi and Phi Kappa Phi Scholastic Honor Societies.

BORMIN HUANG received the Ph.D. degree in satellite remote sensing from the University of Wisconsin–Madison, in 1998. He is currently the Director of the Intel Parallel Computing Center, University of Wisconsin–Madison, a Research Professor with the University of Las Palmas de Gran Canaria, Las Palmas, Spain, a Professor with the School of Information Science and Technology, Southwest Jiaotong University, China, and a Guest Professor with several universities in China. His research interests include remote sensing, satellite data compression, artificial intelligence, and high-performance parallel computing. He is also an NVIDIA CUDA Fellow and a SPIE Fellow. He serves as an Associate Editor for the IEEE JOURNAL OF SELECTED TOPICS IN APPLIED EARTH OBSERVATIONS AND REMOTE SENSING.